PERGAMON

International Journal of Heat and Mass Transfer 42 (1999) 3673–3693

International Journal of HEAT and MASS TRANSFER

www.elsevier.com/locate/ijhmt

A direct numerical simulation of natural convection between two infinite vertical differentially heated walls scaling laws and wall functions

T.A.M. Versteegh, F.T.M. Nieuwstadt*

J.M. Burgers Centre, Delft University of Technology, Rotterdamseweg 145, 2628 AL Delft, The Netherlands

Received 11 March 1998; received in revised form 16 November 1998

Abstract

A direct numerical simulation has been performed for the case of a natural convection flow between two differentially heated vertical walls for a range of Rayleigh numbers ($5.4 \times 10^5 < Ra < 5.0 \times 10^6$). The simulation data are compared with experimental data of Dafa'Alla and Betts [Experimental study of turbulent natural convection in a tall cavity, Exp. Heat Transfer 9 (1996) 165–194] and the agreement is found to be acceptable. Given the numerical data we consider the scaling behaviour of the mean temperature, the mean velocity profile and of the profiles of various turbulence statistics. Point of departure is the approach proposed by George and Capp [A theory for natural convection turbulent boundary layers next to heated vertical surfaces, Int. J. Heat Mass Transfer 22 (1979) 813–826] who have formulated scaling relationships valid, respectively, in the near-wall inner layer and in the outer layer in the centre region of the channel. Matching of the scaling relationships in the overlap between the inner and outer region leads to explicit expressions which can be used as wall functions in computational procedures. The DNS data confirm the results of George and Capp for the scaling of the mean temperature profile. For the mean velocity profile our DNS data support another scaling in terms of a defect law for the velocity gradient in the inner layer. The scaling of George and Capp is also found to apply to the Reynolds stress, the temperature variance and the temperature fluxes. However, the velocity variances again seem to follow a different scaling.

1. Introduction

Turbulence can be characterized in terms of its production process, the most important ones in practice being shear and buoyancy. The physics and consequences of these production processes are best studied in a simple flow geometry to avoid other disturbing influences. An example of such a simple flow geometry is given by two parallel infinite walls and it is denoted as a channel or duct. The advantage of studying turbulence in this geometry is that all flow statistics depend only on the coordinate perpendicular to the wall and are independent of the other two directions. Shear flow in a channel has, for instance, been studied by a number of authors, e.g. Antonia et al. [1] by means of experiment and numerical simulation. In this paper we concentrate on the other production process, i.e. buoyancy, where a flow dominated by buoyancy production is called natural convection.

To study turbulence production by buoyancy in a channel geometry one has to specify the direction of

* Corresponding author.

E-mail address: j.nieuwstadt@wbmt.tudelft.nl (F.T.M. Nieuwstadt)

0017-9310/99/$ - see front matter
PII: S0017-9310(99)00037-X

Nomenclature

f_t	horizontal temperature flux
g	acceleration of gravity
h	channel width
H	modified Rayleigh number
L_x, L_y, L_z	size of computational domain in the x-, y- and z-direction
N_x, N_y,N_z	number of grid points in the x-, y- and z-direction
Nu	Nusselt number
Pr	Prandtl number
Ra	Rayleigh number
T	temperature
u	velocity component along the x-axis
v	velocity component along the y-axis
w	velocity component along the z-axis
w_i	inner velocity scale
w_o	outer velocity scale
x	coordinate direction perpendicular to walls
y	coordinate direction in the horizontal direction parallel to the wall
z	coordinate direction in the vertical direction parallel to the wall

Greek symbols

β	volumetric expansion coefficient
ΔT	temperature difference between the two walls
κ	heat diffusion coefficient
ν	kinematic viscosity

gravity with respect to the channel wall. The most familiar case is when gravity is perpendicular to the walls. The flow is then denoted as Rayleigh–Bénard convection. The other case is for gravity parallel to the wall. A natural convection flow results in this geometry when the two walls are kept at a different temperature. For small temperature differences the flow is laminar and when a certain critical value [2] is exceeded, the flow becomes turbulent. Here, we will turn to this latter case of a turbulent natural convection flow between two vertical, differentially heated walls. It has been relatively little studied, in comparison with the case between horizontal walls [3].

This flow geometry is interesting from a practical point of view because it is relevant for problems involving heat transfer from a vertical wall. Examples are heating and cooling of building spaces, insulation properties of double paned windows or cooling of electronic components. However, the problem is also interesting from a fundamental point of view. For instance, in contrast to the more familiar Rayleigh–Bénard convection a mean flow develops which complicates the turbulence dynamics due to the additional effect of turbulence production by shear. Although this may perhaps be interpreted as the flow being influenced by both buoyancy and shear, we shall nevertheless remain with our characterization as pure natural convection because the mean flow is the direct result of buoyancy. A perhaps interesting fact to note here is that the turbulence production by shear occurs in the same direction as the buoyant production. In most other flows where both buoyant and shear production play a role, the two processes usually act in different directions.

In view of experiments it should be mentioned that our two plate geometry is of course idealized and it cannot be realized in the laboratory. Nevertheless, observational studies on related geometries are available. First of all, these are the studies carried out in tall cavities as reported by Elder [4], Betts and Dafa'Alla [5] and Dafa'Alla and Betts [6]. Another related geometry is a single, vertically heated wall on which experimental studies have been carried out by Cheesewright [7] and Tsuji and Nagano [8–10]. The channel geometry can easily be represented by numerical simulations of turbulence. Numerical studies of this problem have been reported by Phillips [11] and by Boudjemadi et al. [12]. In the present investigation we shall also make use of numerical simulation. In particular we shall use Direct Numerical Simulation (DNS) in which all turbulent flow motions are resolved and no modelling assumptions are made.

The results of DNS in comparison with experimental

data have an advantage, they lead to more complete information on the flow at hand and also usually lead to more accurate statistics. The latter property is in particular, useful for the present study where we concentrate on the scaling behaviour of the mean flow and turbulence quantities. Scaling is a well-established method to study turbulent and perhaps the most well-known example is the scaling of near-wall turbulent shear flow. Here, one distinguishes between an inner layer which depends on wall characteristics and an outer layer which depends on the general flow geometry. In each region scaling laws can be formulated and these require matching in an overlap region between the inner and outer layer. As a direct consequence of matching an explicit expression for the velocity and temperature profile follows: the well-known logarithmic profile. This profile is sometimes also denoted as a wall function because it can be used in computations to prescribe the velocity function near the wall. For some recent views on this scaling of near-wall shear flow we refer to Bradshaw and Huang [13].

Scaling has also been applied to natural convection flow. In the Rayleigh–Bénard convection an approach in terms of an inner and outer layer has been considered. Matching leads again in this case to an explicit expression for the temperature profile [14]. The resulting profile seems to agree with laboratory experiments but not with atmospheric data [15]. Another result following from this scaling is an explicit relationship between the Nusselt (Nu) and Rayleigh (Ra) numbers following $Nu \sim Ra^{1/3}$. Such an expression seems indeed to be observed for relatively small Rayleigh numbers but at higher Rayleigh numbers it has been argued that the exponent in this heat transfer law changes to 2/7 [16].

Scaling of a turbulent natural convection flow along a vertical wall has been hardly explored. The only systematic study is reported by George and Capp [17] who again propose a scaling in terms of an inner and outer layer. The resulting scaling relationships or the wall functions which follow from matching both layers, seem to agree with measurements for the mean temperature profile but not for the velocity profile. In several other studies [18,19] the existence of wall functions, in particular for the mean velocity, has been considered without finding a completely satisfactory result. Nevertheless, for practical applications wall functions would be very useful because their application in numerical computations avoids explicit computation of the near-wall temperature and velocity profile. Namely, both the temperature and velocity have a large gradient in the neighbourhood of the wall and the need to resolve this gradient would be computationally, very expensive. Furthermore, the use of a wall function enforces correct behaviour for the heat transfer which is obviously important for practical applications.

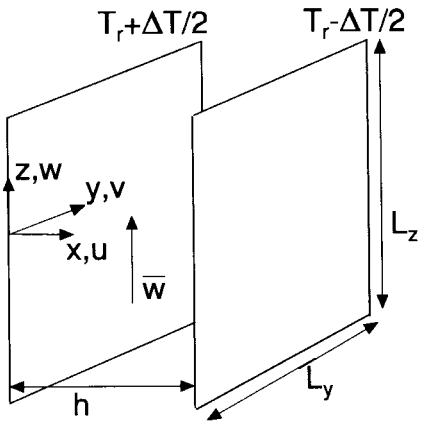

Fig. 1. Flow geometry and definition of the coordinate system.

In view of the discussion given above, it is our objective to continue the study on the scaling of turbulent natural free convection in the neighbourhood of a vertical wall. The point of departure is the scaling approach in terms of an inner and outer layer first explored by George and Capp [17]. The availability of our DNS results allows a fresh approach which may be explored in order to produce new insight in the scaling behaviour of this flow. Using the DNS data we aim to formulate inner- and outer-layer scaling expressions for the mean temperature and velocity profile and also for various turbulence quantities. Furthermore, based on the matching of these scaling relationships, we shall attempt to derive wall functions.

The outline of this paper is as follows: in the next section the governing equations and their solution with DNS is discussed. In the following section we consider the results of the DNS and compare these with experimental data. In the sections thereafter, we explore the scaling of the DNS data. First, we will select the appropriate scaling parameters in each region. Based on these parameters we will then consider the scaling of various variables and the consequences. We end this study with some conclusions.

2. Basics

2.1. Flow geometry and governing equations

A schematic illustration of the flow geometry is given in Fig. 1. The distance between the two walls is h and the temperature difference ΔT. The kinematic viscosity ν, the heat diffusion coefficient κ and the volumetric expansion coefficient β are fluid properties.

Table 1
Computational details of the DNS-simulations of the free convection flow between two infinite, differentially heated, vertical walls

Computational domain	$L_z \times L_y \times L_x = 12\ h \times 6\ h \times h$
Number of grid points (coarse resolution)	$N_z \times N_y \times N_x = 180 \times 90 \times 48$
Number of grid points (fine resolution)	$N_z \times N_y \times N_x = 432 \times 216 \times 96$
Min/max cell in x-direction (coarse resolution)	$\Delta x_{\min} = 0.000975h$, $\Delta x_{\max} = 0.00292h$
Min/max cell in x-direction (fine resolutions)	$\Delta x_{\min} = 0.000439h$, $\Delta x_{\max} = 0.00131h$

The origin of the x-coordinate is put on the left wall so that the centre of the channel is given by $x = h/2$. As a result of the boundary conditions, the mean temperature and velocity profile are antisymmetric with respect to the plane $x = h/2$. The derivatives of these profiles and also the turbulent fluxes and variances are symmetrical with respect to the same plane. Therefore, it will be sufficient to present only results for the region given by $0 < x < h/2$. The z-coordinate is chosen in the vertical direction, i.e. along the direction of gravity. The y-coordinate lies in the spanwise direction. The temperature is denoted by T and the velocity components along the x-, y- and z-directions by u, v and w, respectively.

The natural convection flow is driven by the temperature difference ΔT in combination with the acceleration of gravity g. Given these variables and the parameters introduced above, we can define a dimensionless parameter which characterizes the flow and which is known as the Rayleigh number

$$Ra = \frac{g\beta\Delta T h^3}{\nu\kappa}. \tag{1}$$

It will turn out that a more convenient parameter in our study is the 'modified' Rayleigh number, H, which is defined as

$$H = Pr\ Ra = \frac{g\beta\Delta T h^3}{\kappa^2} \tag{2}$$

where the Prandtl number Pr is defined as

$$Pr = \frac{\nu}{\kappa}. \tag{3}$$

We also introduce the Nusselt number which can be interpreted as the non-dimensional temperature flux. Its definition reads

$$Nu = \frac{f_t h}{\Delta T \kappa}. \tag{4}$$

Here, f_t is the horizontal temperature flux defined as

$$f_t = \kappa \left.\frac{\partial T}{\partial x}\right|_0 \tag{5}$$

where the differential $\partial T/\partial x$ is evaluated at the wall as indicated by the index 0.

In the following we shall use dimensionless variables, unless explicitly mentioned otherwise. To non-dimensionalize all physical variables we employ the parameters ΔT, h and κ. The governing equations in terms of non-dimensional variables read

$$\frac{\partial u_i}{\partial x_i} = 0$$

$$\frac{\mathrm{D}u_i}{\mathrm{D}t} = H(T - T_r)\delta_{i3} + Pr\frac{\partial^2 u_i}{\partial x_j^2}$$

$$\frac{\mathrm{D}T}{\mathrm{D}t} = \frac{\partial^2 T}{\partial x_j^2} \tag{6}$$

where T_r is a reference temperature equal to the average temperature between the two walls. It then follows that the vertical velocity averaged over an arbitrary horizontal plane, i.e. $0 < x < h$ and $0 < y < L_y$, becomes zero. The temperature difference, $T - T_r$, contributes only to the equation for the vertical velocity component as enforced by the Kronecker delta δ_{i3} in (6). We have used the Boussinesq approximation, i.e. the flow can be considered as incompressible and the temperature difference only plays a role in a combination with the acceleration of gravity.

We consider here turbulent flow. In that case each variable can be subdivided in a mean flow (indicated by an overbar[1]) and a fluctuation (indicated by a prime). The mean flow in the channel under the influence of the temperature difference ΔT is stationary and homogeneous in the y- and z-direction. Consequently, all turbulence statistics are functions of the coordinate x only. From (6) it then follows that the equations for the mean flow become

$$0 = g\beta(\bar{T} - T_r) + \frac{\partial}{\partial x}\left(-\overline{u'w'} + \nu\frac{\partial \bar{w}}{\partial x}\right) \tag{7}$$

[1] In the figures the notation of an average will be given by angular brackets with the exception of the mean vertical velocity which will be denoted by an upper case letter.

$$0 = \frac{\partial}{\partial x}\left(-\overline{u'T'} + \kappa\frac{\partial \bar{T}}{\partial x}\right). \tag{8}$$

2.2. DNS

The set of Eqs. (6) is solved numerically in a computational domain in the form of a rectangular box. The size of the box in the three coordinate directions is given in Table 1. We have found that the numerical results depend on this size. For instance, computations with a domain size of $L_z \times L_y \times L_x = 2.5h \times 1.0h \times 1.0h$, which was used by Boudjemadi et al. [12], lead to differences in comparison with the results for our larger domain. For instance, the mean velocity in our case was found to be smaller than the values obtained by Boudjemadi et al. [12]. However, when we adopted the same size of the computational domain, our results turned out to be exactly equal to those of Boudjemadi et al. [12]. This latter fact may also be considered to be an independent test for the correctness of our numerical code.

On the computational domain mentioned above, a Cartesian grid is introduced. In the y- and z-direction a constant grid spacing is used. In the horizontal x-direction the grid spacing is variable with the minimum size near the wall and the maximum size near the centreline. The computations have been carried out with a coarse and fine grid (see Table 1 for details). In Versteegh [20] it has been estimate that the fine grid is sufficient to resolve all flow scales for $Ra \leqslant 5 \times 10^6$ which sets the largest Rayleigh number that we can compute with our DNS.

The numerical technique that we have used, is a finite volume scheme with a second-order discretization method for both the non-linear advection and the linear diffusion terms. The time-stepping method is the explicit Adams–Bashford method which is second-order in time. The constraint of continuity is imposed by means of the pressure correction method. This method leads to a Poisson equation for the pressure which is solved by a Fast-Fourier method in the homogeneous y- and z-direction and a finite difference method in the inhomogeneous x-direction. As mentioned above, we have performed our DNS on two grids. By combination of the results from both grids with the help of the so-called Richardson extrapolation, we can obtain a more accurate solution which in theory can reach fourth-order (on a uniform grid and for a sufficiently smooth solution). In Versteegh [20] it is discussed that in our case Richardson's extrapolation leads to higher accuracy than second order.

For the boundary conditions on the two vertical walls we employ no-slip conditions for the velocity and a constant value for the temperature. In the homogeneous y- and z-direction periodic conditions are applied. In view of our limited domain in these directions this boundary condition is only acceptable when the largest turbulence scales are smaller than about half the domain size. This requirement has been checked by computation of the correlation functions in the y- and z-directions and these were indeed found to drop to small values over a distance of half the domain size.

Table 2
The Rayleigh and modified Rayleigh number of the four simulations together with the symbol for each computation that will be used in the following figures

Ra	H	Symbol
5.4×10^5	3.829×10^5	○
8.2×10^5	5.833×10^5	△
2.0×10^6	1.418×10^6	□
5.0×10^6	4.254×10^6	▽

Simulations have been performed for four values of the Rayleigh number given in Table 2. The choice for the largest Rayleigh number is set by the grid size as discussed above. The lowest Rayleigh number has been chosen equal to the value used by Boudjemadi et al. [12] so that comparison with their results can be carried out. The remaining two Rayleigh numbers have been chosen to cover the interval between $Ra = 5.4 \times 10^5$ and $Ra = 5 \times 10^6$. Furthermore, they are close to the values of the Rayleigh number used in the experiments of Dafa'Alla and Betts [6]. In all cases the Prandtl number is taken equal to $Pr = 0.709$.

In the following we will only present results of turbulence statistics. For results on the instantaneous flow and temperature field, for instance in terms of coherent structures, we refer to Versteegh and Nieuwstadt [21]. Statistics of the simulation data are computed by means of taken an average over the y- and z-plane. Given the periodic boundary conditions in these directions, it can be shown that this average has the same properties as an ensemble average. Therefore, the numerical average can be interpreted as being similar as the average applied in (7) and (8) and consequently it is again indicated by an overbar.

3. DNS results and comparison with experimental data

In this section we will present the results from our DNS and compare these with the experimental data of Dafa'Alla and Betts [6]. Let us first discuss some details of the experimental data. The experiments have been carried out in a tall cavity with a vertical length of $L_z/h = 28.6$ and a width of $L_y/h = 6.8$. The spacing between the two walls is $h = 0.076$ m. The working medium is air. Results have been obtained for two

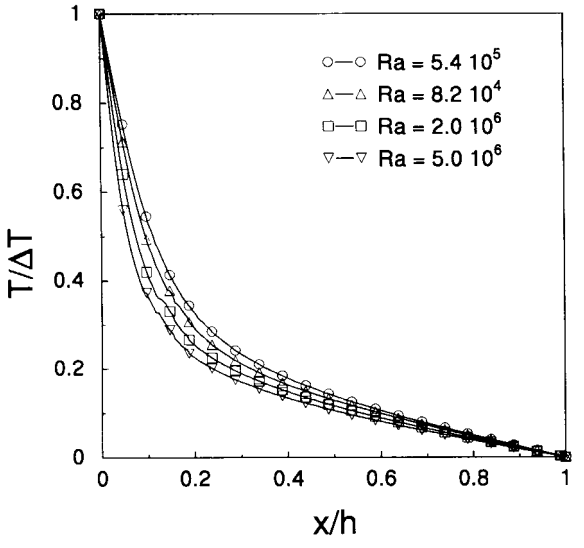

Fig. 2. The mean temperature profiles obtained from the DNS data for the four values of the Rayleigh number.

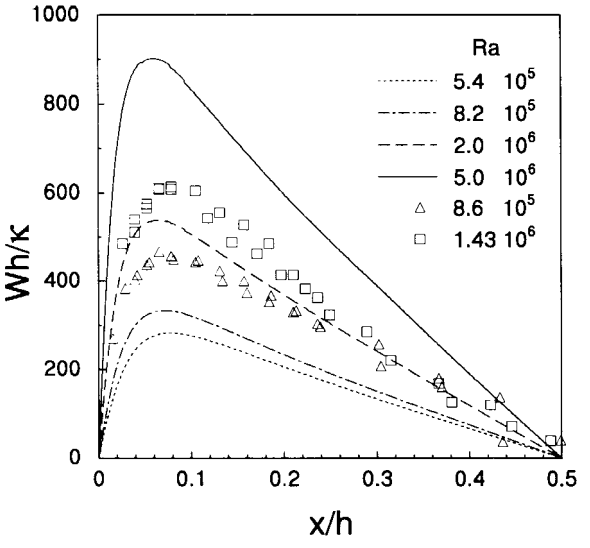

Fig. 4. The mean velocity profiles obtained from the DNS data (lines) and the experimental data (symbols) for four, respectively two, values of the Rayleigh number.

values of the temperature difference ΔT, i.e. 19.6 and 39.1°C, for which the Rayleigh numbers become $Ra = 8.6 \times 10^5$ and $Ra = 1.43 \times 10^6$, respectively. Temperatures are measured with the help of a thermocouple with an accuracy of 0.1°C and a response time of 0.065 s. A Laser Doppler Velocimetry (LDV) system is used to measure velocities. All data presented here, have been obtained in the mid-region of the cavity, i.e. halfway between the length L_z and width L_y.

In Fig. 2 we show the DNS data for the mean temperature profile for the four values of the Rayleigh number. We observe that for the increasing Rayleigh number the temperature profile develops a thinner boundary layer along the wall. In Fig. 3 the DNS data are compared with the experimental observations and the agreement can be called quite reasonable.

The DNS data for the mean velocity profile are shown together with the experimental data in Fig. 4. It is clear that the mean velocity depends strongly on the Rayleigh number with the maximum velocity becoming larger for the increasing Rayleigh number. The agree-

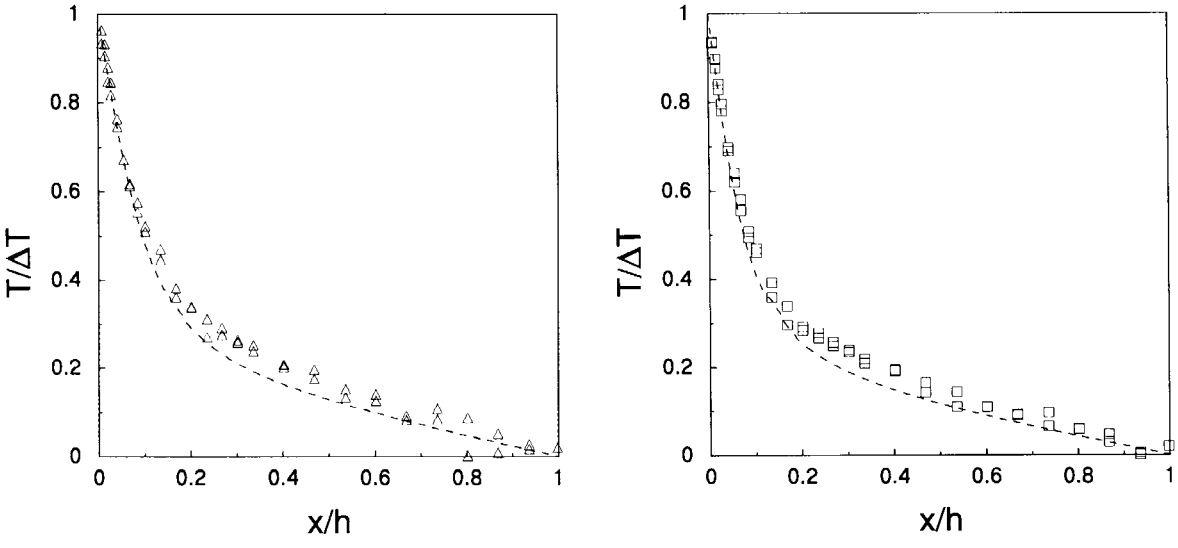

Fig. 3. Comparison of the DNS data (dashed line) with the experimental data (symbols) for $Ra_{DNS} = 8.2 \times 10^5$ and $Ra_{Exp} = 8.6 \times 10^5$ (left figure) and for $Ra_{DNS} = 2 \times 10^6$ and $Ra_{Exp} = 1.43 \times 10^6$ (right figure).

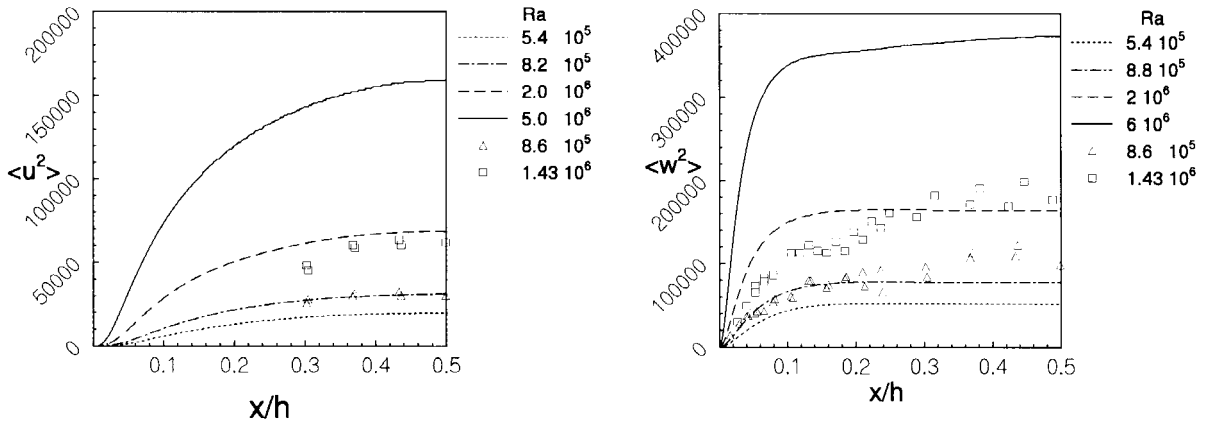

Fig. 5. The variance of the velocity fluctuations in the x-direction (left) and in the z-direction (right) for the DNS data (lines) and the experimental data (symbols) for different values of the Rayleigh number.

ment between the DNS data and experimental results in this case, can be called correct, only qualitatively, i.e. the experimental velocities also increase when the Rayleigh number becomes larger and the maximum value of the velocity occurs at about the same x-location. However, the experimental velocities are considerably larger than the numerical results and for this deviation a suitable explanation is not available.

Next we consider the variances of the turbulent velocity fluctuations. Experimental data are only available for the vertical component, i.e. $\overline{w'^2}$, and for the horizontal component along the x-direction, i.e. $\overline{u'^2}$. The results are shown in Fig. 5. The agreement between the numerical and experimental data can again be called quite reasonable.

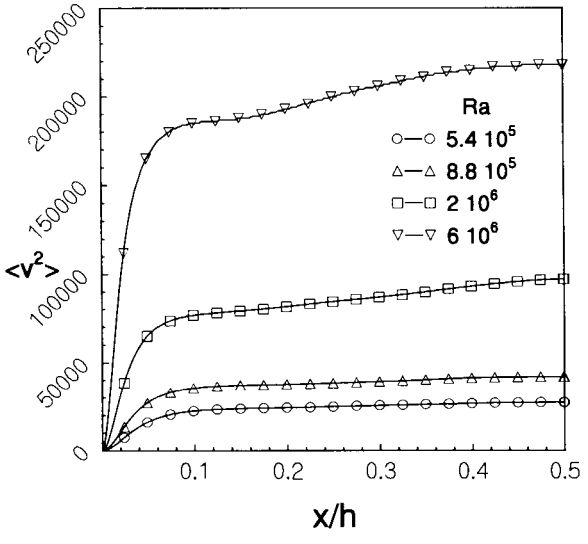

Fig. 6. The various of the velocity fluctuations in the y-direction computed for the DNS data for four values of the Rayleigh number.

Let us now consider the variables for which only numerical data are available. The first is the variance of the other horizontal velocity component which is shown in Fig. 6. A perhaps more interesting variable is the Reynolds stress which is given in Fig. 7, where we find that similar as for the mean velocity profile, the Reynolds stress is a strong function of the Rayleigh number. However, the most interesting result is the behaviour of the Reynolds stress near the wall which is also shown in Fig. 7 by means of an enlargement. It appears that the Reynolds stress is negative only very close to the wall, but that it changes to a positive value near $x \simeq 0.015$. On the other hand Fig. 4 shows that the mean velocity gradient changes sign near $x \simeq 0.7$. Let us assume for the moment that the gradient transfer hypothesis for the Reynolds stress holds, which reads

$$-\overline{u'w'} = K\frac{\partial \bar{w}}{\partial x}.$$

The near-wall behaviour mentioned above of the Reynolds stress and of the mean velocity profile, implies now that the exchange coefficient K must be negative for $\sim 0.015 < x < \sim 0.7$. From a physical point of view the concept of an exchange coefficient which implies transport down the gradient, only makes sense when the exchange coefficient is larger than zero. The conclusion must, therefore, be that the gradient transfer hypothesis cannot be valid in this near-wall region. The consequence is that all modelling approaches for this flow which are based on a gradient-transfer hypothesis, are fundamentally incorrect. Such a gradient-transfer approach was, for example, used by Henkes and Hoogendoorn [18] to derive wall functions for the mean velocity.

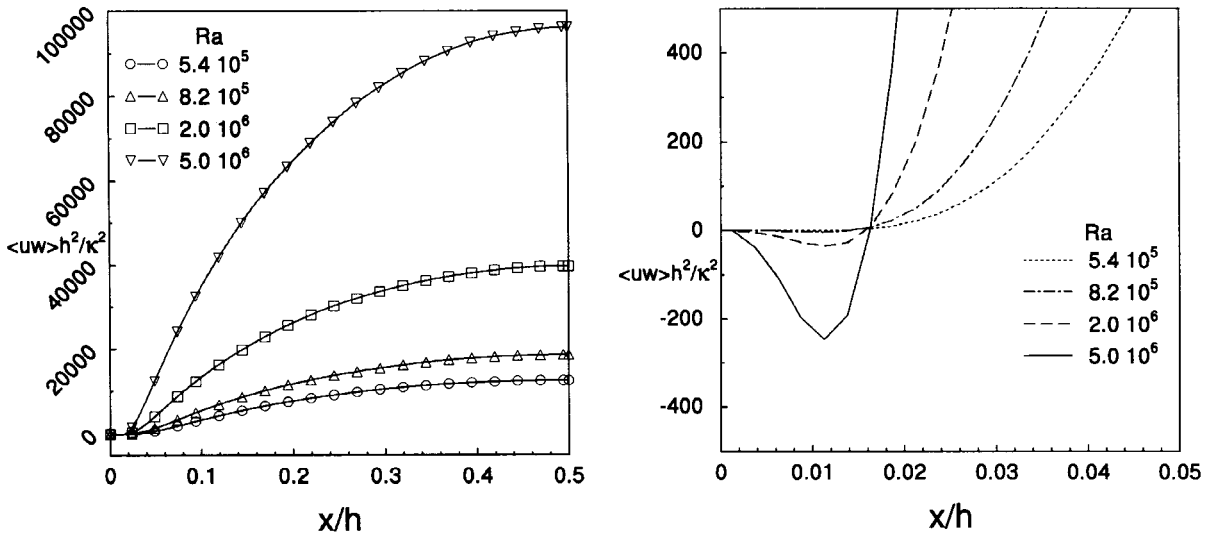

Fig. 7. The Reynolds stress obtained from the DNS data for the four values of the Rayleigh number (left) with an enlargement of the Reynolds stress near the wall (right).

Another consequence of this behaviour of the Reynolds stress is that the turbulence production by shear becomes negative in the near-wall region. In other words the turbulence feeds energy to the mean flow. The maintenance of turbulence itself must thus rely on other processes. Data on the energy budget as presented by Boudjemadi et al. [12] and Versteegh and Nieuwstadt [22] show that apart from buoyancy production transport of turbulence from the centre region is a major source of turbulence in the wall region. This result for the near-wall energy budget is quite different from the other cases of near-wall turbulence.

4. Scaling of mean profiles

4.1. Scaling parameters

In this section we introduce the scaling parameters that we will use to put the various statistical quantities in their non-dimensional similarity form. We start with the assumption first adopted by George and Capp [17] that we can distinguish between an inner and outer layer. The inner layer must be characterized by a parameter which describes the flow condition close to the wall and which is independent of the (large scale) flow geometry. It seems most obvious to select as this parameter, the heat diffusion coefficient κ. In the outer layer in fully developed turbulence the parameter κ should by definition, not play a role. Here, the flow geometry is the determining factor and therefore, we select the channel width h as the characteristic parameter in this region.

Next, we need a parameter that can characterize the production of turbulence by buoyancy. Let us consider the equation for the mean temperature given in (8). This equation can be integrated once with as a result

$$f_t = -\overline{u'T'} + \frac{\partial \bar{T}}{\partial x} \tag{9}$$

where f_t is the horizontal temperature flux (>0) which is representative for the heat flux flowing from the left-hand to the right-hand wall. Eq. (9) implies that this horizontal temperature flux consists of a turbulence and molecular contribution and that it is constant, i.e. $\neq f(x)$. Consequently, f_t seems to be a parameter which is relevant everywhere in the flow and therefore, we select f_t as a characteristic scaling parameter. It should be mentioned that f_t has also been proposed by George and Capp [2] as a scaling parameter.

Table 3
Velocity, temperature and length scale for the inner and outer layer based on the characteristic parameters $g\beta$, f_t, κ and h

	Scaling parameter	Non-dimensional form
Inner layer		
Velocity	$w_i=(g\beta f_t\kappa)^{1/3}$	$(w_ih/\kappa)=(Nu\ H)^{1/4}$
Temperature	$T_i=f_t/w_i$	$(T_i/\Delta T)=Nu/(Nu\ H)^{1/4}$
Length	$l_i=\kappa/w_i$	$(l_i/h)=(Nu\ H)^{-1/4}$
Outer layer		
Velocity	$w_o=(g\beta f_t h)^{1/3}$	$(w_o/\kappa)=(Nu\ H)^{1/3}$
Temperature	$T_o=f_t/w_o$	$(T_o/\Delta T)=Nu/(Nu\ H)^{1/3}$
Length	$l_o=h$	

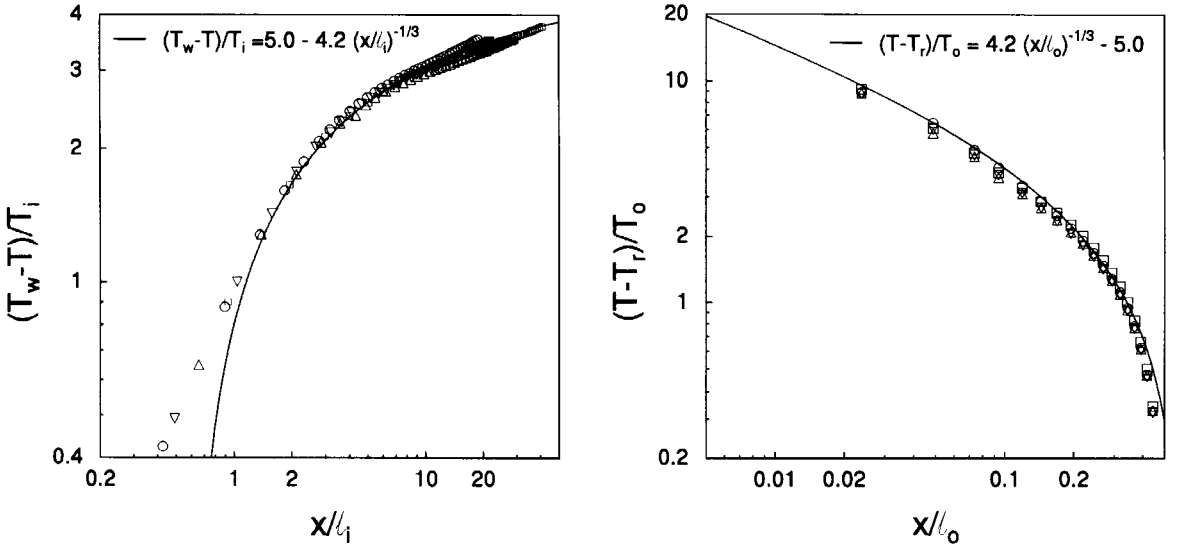

Fig. 8. DNS data for the temperature profile in inner-layer scaling (left) and outer-layer scaling (right); the solid lines give the matching result mentioned in the text; the meaning of the symbols is given in Table 2.

Finally, to complete our selection of scaling parameters we choose the buoyancy parameter $g\beta$ which can be considered as the parameter that is characteristic of the fluid medium.

Based on the parameters introduced above, we can define a velocity, temperature and length scale for the inner and outer layer. The results are summarized in Table 3.

4.2. Scaling of the mean temperature profile

With the help of the scaling parameters introduced in the previous section, we can formulate scaling relationships valid for the inner and outer layer. The result reads

$$\frac{T_w - T}{T_i} = f_T\left(\frac{x}{l_i}\right) \tag{10}$$

$$\frac{T - T_r}{T_o} = F_T\left(\frac{x}{h}\right) \tag{11}$$

where the notation f_T and F_T has been used to indicate unknown functional relationships which cannot be obtained from the scaling analysis and which should for instance follow from experiments. We note that in each region a formulation in terms of a temperature defect law has been adopted.

Next we assume that both scaling laws remain valid in an overlap region between the inner and outer layer. In this overlap region both expressions (10) and (11) should match. In view of the formulation in terms of a defect law, we can perform the matching procedure only on the temperature gradient. A matching condition as for instance outlined in Tennekes and Lumley [23], takes the form

$$\lim_{x/l_i\to\infty} -\frac{T_i}{l_i} f'_T\left(\frac{x}{l_i}\right) = \lim_{x/h\to 0} \frac{T_o}{h} F'_T\left(\frac{x}{h}\right).$$

With the help of the identity

$$\frac{T_i}{T_o} = \left(\frac{h}{l_i}\right)^{1/3}$$

which follows from the results given in Table 3 and given the fact that at the same time the limit $h/l_i \to \infty$ should be satisfied, we find the following matching condition

$$-\left(\frac{x}{l_i}\right)^{4/3} f'_T\left(\frac{x}{l_i}\right) = \left(\frac{x}{h}\right)^{4/3} F'_T\left(\frac{x}{h}\right) = -c_1$$

which c_1 is a constant. Integration then leads to the following expressions for the temperature profile in the overlap region

$$\frac{T_w - T}{T_i} = -c_1\left(\frac{x}{l_i}\right)^{-1/3} + A_1 \tag{12}$$

$$\frac{T - T_r}{T_o} = c_1\left(\frac{x}{h}\right)^{-1/3} + B_1 \tag{13}$$

where A_1 and B_1 are two integration constants.

In Fig. 8 we have plotted the DNS data in terms of inner and outer layer scaling. In the same figure we

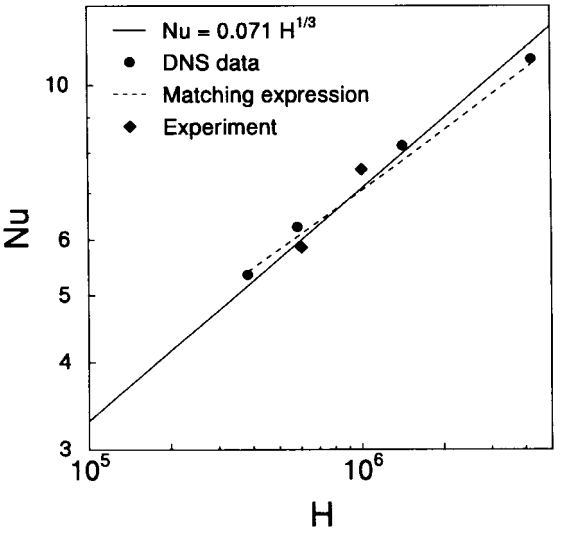

Fig. 9. The Nusselt number versus the modified Rayleigh number; the closed circles denote the DNS data and the closed diamond the experimental data of Dafa'Alla and Betts [6]; the dashed line follows from an expression obtained by matching the temperature profile in the inner and outer layer; the solid line gives a best fit in terms of the expression $Nu \simeq H^{1/3}$.

also show the expressions (12) and (13). It is clear that all DNS data conforms excellently to both inner- and outer-layer scaling. Moreover, the expressions (12) and (13) with $c_1 = 4.2$ and with $A_1 = 5.0$ and $B_1 = -5.0$ form a very good fit to the data.

A further result can be obtained from the matching expressions (12) and (13) by adding both equations after multiplication with T_i and T_o, respectively. This leads to the following result

$$Nu^{3/4}\left[1 + \frac{B_1}{A_1}(Nu \cdot H)^{-1/12}\right] = \frac{1}{2^* A_1} H^4 \tag{14}$$

which can be interpreted as a heat transfer law.

In Fig. 9 the DNS data for the Nu and H are shown in comparison with the expression (14) with $A_1 = -B_1 = 5.0$. It is clear that the matching expression agrees excellently with the DNS data which in our opinion confirms the consistency of our outer- and inner-layer scaling approach of the temperature. We also show in Fig. 9 a fit to the data in terms of power law given by

$$Nu = 0.071 H^{1/3}.$$

Such an expression is frequently used as a heat transfer law in practice. It is clear that this power law given an equally good approximation to the data as the results of the theoretical expression (14). In this respect we note that when H and consequently also Nu increase, the expression (14) reduces to such a 1/3-power law. Finally, it should be mentioned that the experimental data of Dafa'Alla and Betts [6] are also given in Fig. 9 and they agree excellently with the DNS results.

4.3. Scaling of the mean velocity profile

From the equation of motion (7) it follows that the mean velocity profile is directly connected to the Reynolds stress $u'w'$. Therefore, we begin this section

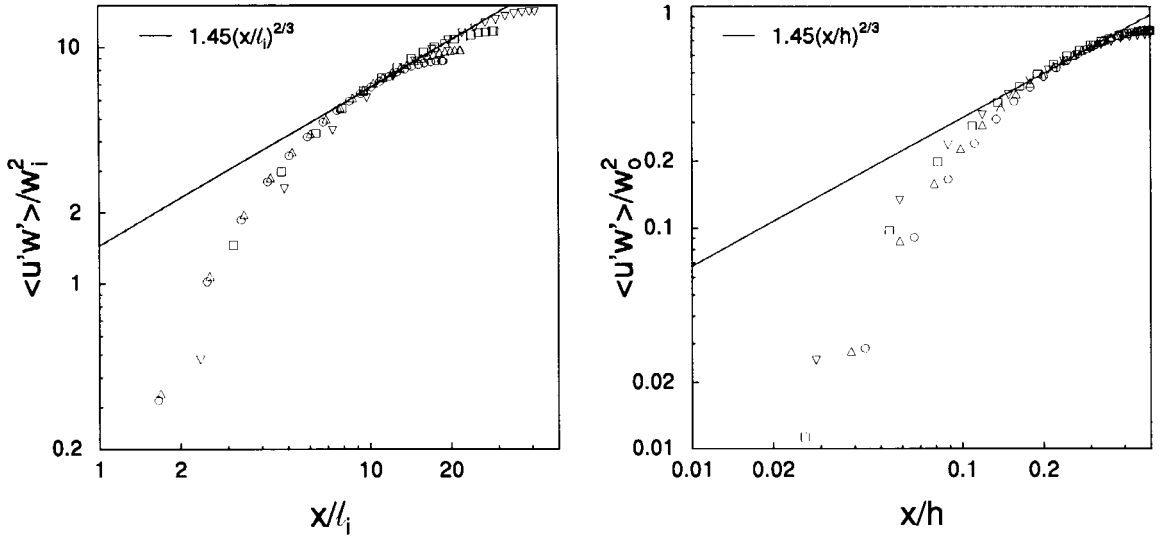

Fig. 10. DNS data for the Reynolds-stress profile in inner-layer scaling (left) and outer-layer scaling (right); the dashed lines give the matching result mentioned in the text; the meaning of the symbols is given in Table 2.

on the scaling of the mean velocity profile by first considering the scaling of the Reynolds stress.

Let us assume that the Reynolds stress follows the same inner- and outer-layer scaling as we have found to be valid for the temperature profile. This assumptions seems reasonable because apart from connecting the Reynolds stress with the mean velocity profile (7) it also connects the Reynolds stress with the mean temperature profile. The following scaling relationships for the inner and outer layer should hold

$$\frac{\overline{u'w'}}{w_\mathrm{i}^2} = g_{uw}\left(\frac{x}{l_\mathrm{i}}\right) \tag{15}$$

$$\frac{\overline{u'w'}}{w_\mathrm{o}^2} = G_{uw}\left(\frac{x}{h}\right) \tag{16}$$

where the velocity and length scales are the same as defined in Table 3. The results for the inner- and outer-layer scaling of the $\overline{u'w'}$ are shown in Fig. 10. Comparing these scaling results with the original shear stress profiles given in Fig. 7, we find that the inner- and outer-scaling is indeed able to collapse the Reynolds stress data reasonably well onto a single curve. Therefore, we venture to conclude that the Reynolds stress obeys standard inner- and outer-layer scaling.

Subsequently, we assume the existence of an overlap region between the inner and outer layer. We can then define a similar matching procedure as has been used for the temperature profile in Section 4.2 with the difference that matching can now be applied directly to the Reynolds stress itself instead of to its gradient. The result of matching is again an explicit expression for the Reynolds stress which in inner and outer scaling reads

$$\frac{\overline{u'w'}}{w_\mathrm{i}^2} = c_2\left(\frac{x}{l_\mathrm{i}}\right)^{2/3} \tag{17}$$

$$\frac{\overline{u'w'}}{w_\mathrm{o}^2} = c_2\left(\frac{x}{h}\right)^{2/3}. \tag{18}$$

These relationships are also shown in Fig. 10 with the value 1.45 for the constant c_2. A reasonable agreement is found between the scaling laws and the matching expression between $7 < x/l_\mathrm{i} < 15$ or $0.15 < x/h < 0.3$.

Having established the scaling for the Reynolds stress, we now consider the scaling of the mean velocity profile. As already mentioned above, the mean velocity and the Reynolds stress are connected through the equation of motion (7). Therefore, we first investigate the consequences of this equation. Integrating between 0 and x we find

$$0 = H\int_0^x (\bar{T} - T_\mathrm{r})\,\mathrm{d}s - \overline{u'w'}(x) + Pr\left(\frac{\mathrm{d}\bar{w}}{\mathrm{d}x} - \left.\frac{\mathrm{d}\bar{w}}{\mathrm{d}x}\right|_0\right)$$

where s denotes an integration variable. We have used the boundary condition $u'w'(0)=0$. The $\mathrm{d}\bar{w}/\mathrm{d}x|_0$ is the velocity gradient at the wall. Performing a second integration leads to

$$0 = H\int_0^x (x-s)(\bar{T} - T_\mathrm{r})\,\mathrm{d}s - \int_0^x \overline{u'w'}(s)\,\mathrm{d}s + Pr\left(\bar{w}(x) - \left.\frac{\mathrm{d}\bar{w}}{\mathrm{d}x}\right|_0 x\right). \tag{19}$$

If we evaluate the latter equation at $x=0.5$ and substitute the symmetry condition for the velocity $\bar{w}(0.5)=0$, we find the following relationship for the velocity gradient at the wall

$$u_*^2 \equiv Pr\left.\frac{\mathrm{d}\bar{w}}{\mathrm{d}x}\right|_0 = 2\left[H\int_0^{1/2}\left(\frac{1}{2}-s\right)(\bar{T} - T_\mathrm{r})\,\mathrm{d}s - \int_0^{1/2}\overline{u'w'}(s)\,\mathrm{d}s\right]. \tag{20}$$

Here u_* is the (non-dimensional) friction velocity which is defined as

$$u_*^2 = \frac{\tau_\mathrm{o} h^2}{\rho\kappa^2}$$

with τ_o the shear stress at the wall.

Eq. (20) is now taken as the point of departure to determine the scaling behaviour of the velocity profile. We first consider the integral of the Reynolds stress in (20). As a result of the inner- and outer-layer scaling found above, we can write the following composite expression for the Reynolds stress

$$\overline{u'w'} = w_\mathrm{i}^2 g_{uw}\left(\frac{x}{l_\mathrm{i}}\right) + w_\mathrm{o}^2 G_{uw}\left(\frac{x}{h}\right) - c_2 w_\mathrm{o}^2\left(\frac{x}{h}\right)^{2/3} \tag{21}$$

where we have dropped our non-dimensional notation. This expression for the Reynolds stress is uniformly valid in the whole channel, i.e. both in the inner and outer layer. The explanation for the third term on the right-hand-side of (21) follows from the fact that the functions g_{uw} and G_{uw} are both, by definition, consistent with matching. Therefore, their sum in (21) would imply that the matching result is taken into account twice and consequently, we must subtract the matching result once. Substitution of this expression in the integral of the (non-dimensional) Reynolds stress leads to

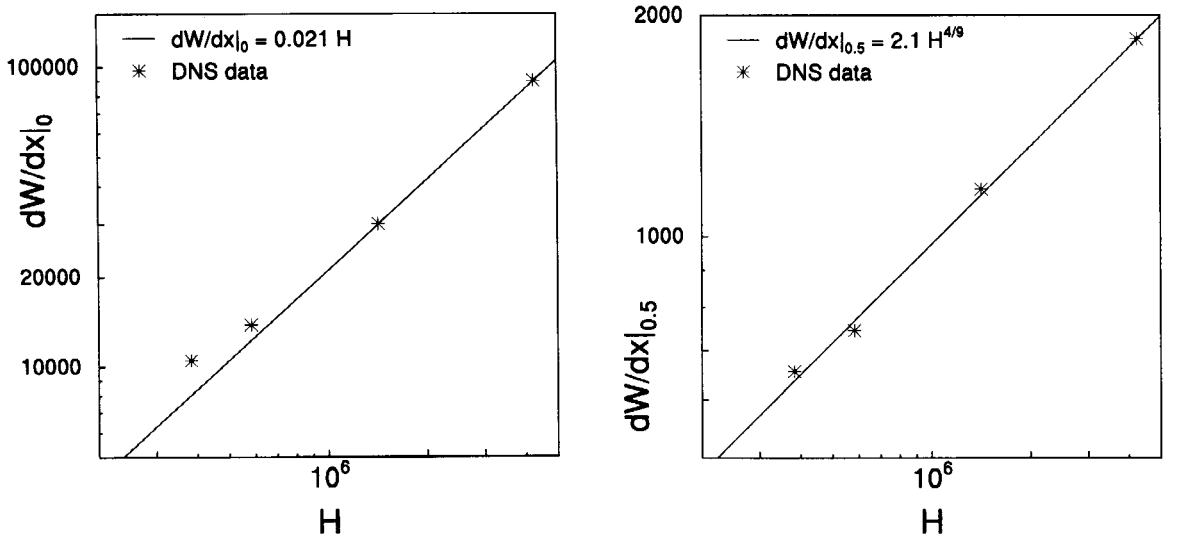

Fig. 11. DNS data for the mean velocity gradient at the wall, i.e. $x=0$ (left) and at the centre of the channel, i.e. $x=0.5$ (right) as a function of H.

$$\int_0^{1/2} \overline{u'w'}(s)\,\mathrm{d}s = (H\,Nu)^{1/4}\int_0^{\infty} g_{uw}(\xi)\,\mathrm{d}\xi + (H\,Nu)^{2/3}\left(\int_0^{0.5} G_{uw}(\eta)\,\mathrm{d}\eta - \frac{3}{5}0.5^{5/3}c_2\right) \tag{22}$$

where we have used Table 3 to transform this expression in non-dimensional form given the profile (21) and where we have set $h/(2\ l_i)\to\infty$ which as follows from Table 3 is the appropriate limit for large values of Ra. The two integrals on the right-hand-side are now, by definition, $O(1)$. With the help of the approximate relationship $Nu\simeq H^{1/3}$, we can then estimate the Reynolds-stress integral as follows

$$\int_0^{1/2} \overline{u'w'}(s)\,\mathrm{d}s \simeq O(H^{1/3}) + O(H^{8/9}) \tag{23}$$

where the first term on the right-hand-side results from the contribution of the inner layer and the second term from the outer-layer contribution. We thus find that the integral of the Reynolds stress is dominated by the contribution of the outer layer.

Next we consider the temperature integral in (20). Using the scaling results for the temperature discussed in Section 4.2, we can again define a composite expression for $\bar{T}$ which is uniformly valid in the channel. In dimensional notation it reads

$$(\bar{T}-T_r) = (T_w - T_r) - T_i f_T\left(\frac{x}{l_i}\right) + T_o\left[F_T\left(\frac{x}{h}\right) - c_1\left(\frac{x}{h}\right)^{-1/3} - B_1\right]. \tag{24}$$

Following the same procedure as for the derivation of (23) we obtain the following estimate for the (non-dimensional) temperature integral

$$H\int_0^{0.5}\left(\frac{1}{2}-s\right)(\bar{T}-T_r)\,\mathrm{d}s \simeq O(H) + O(H^{8/9}). \tag{25}$$

Again the integral can be considered as being made up out of two contributions with the first term on the right-hand-side of (25) resulting from the inner layer and the second term resulting from the outer layer. In this case the contribution from the inner layer seems to dominate, although its deviations from the contribution from the outer layer is small.

Comparison of (23) with (25) shows that the term representative for the outer-layer contribution has the same magnitude in both equations. This result is consistent with a balance between the Reynolds stress and buoyancy effects in the outer layer where viscous effects are, by definition, small. For the inner layer the contribution from the temperature integral is $O(H)$ which is much larger than the contribution from the Reynolds stress integral which is $O(H^{1/3})$. Therefore,

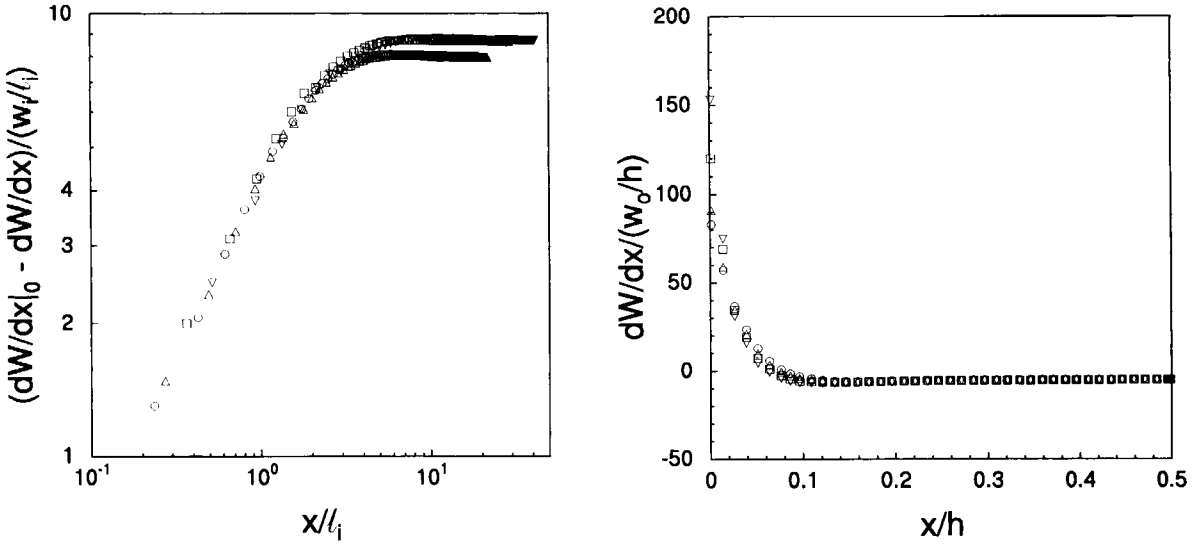

Fig. 12. DNS data for the profile of the mean velocity gradient in inner-layer scaling (left) and outer-layer scaling (right); the meaning of the symbols is given in Table 2.

in the inner region Reynolds stresses cannot balance buoyancy and we must allow a balance between the temperature integral and the viscous stress at the wall which is given by the term on the left-hand-side of (20). However, if the velocity in the inner layer would obey inner-layer scaling, the viscous stress at the wall should scale according to

$$Pr\left.\frac{d\bar{w}}{dx}\right|_0 \simeq Pr\, w_i/l_i = O(Pr\, H^{2/3}).$$

It is clear that for $Pr \simeq O(1)$ such a scaling can never balance a $O(H)$ buoyancy force. The conclusion must be that standard inner-layer scaling cannot be valid for the velocity gradient near the wall. A balance between the viscous and buoyancy term near the wall is only possible when the velocity gradient at the wall scales according to

$$\left.\frac{d\bar{w}}{dx}\right|_0 \sim O(H). \tag{26}$$

To check the scaling estimate given in (26) we plot our simulation results for $d\bar{w}/dx|_0$ as a function of H in Fig. 11 (left). The $d\bar{w}/dx|_0$ seems indeed to follow a linear relationship with H with a constant of proportionality equal to 0.021.

Let us also consider the velocity gradient in the centre of the channel, i.e. at $x=0.5$. If the velocity profile would conform here to standard outer-layer scaling, this would imply

$$\left.\frac{d\bar{w}}{dx}\right|_{0.5} \sim \frac{w_o}{h} \sim O(H^{4/9}). \tag{27}$$

In Fig. 11 (right) we have also plotted this velocity gradient in the centre of the channel which confirms the scaling (27).

To continue our discussion on the scaling of the mean velocity, we note that another restriction to be satisfied is the equation of motion for the mean velocity (7). We have already seen that both the temperature and the Reynolds stress can be scaled in terms of outer- and inner-layer variables. Therefore, (7) implies that the scaling of the second derivative of the mean velocity should also be subdivided in an inner and an outer layer.

Based on this fact and that at the same time the velocity gradient at the wall should satisfy an $O(H)$ scaling, we propose the following similarity form for the velocity gradient

$$\frac{d\bar{w}/dx\,|_0 - d\bar{w}/dx}{w_i/l_i} = f'_w\left(\frac{x}{l_i}\right). \tag{28}$$

To formulate a scaling for the mean velocity profile in the outer layer we use the result given by (27) and illustrated in Fig. 11 (right). Based hereon, we propose for the mean velocity profile in the outer layer

$$\frac{d\bar{w}/dx}{w_o/h} = F'_w\left(\frac{x}{h}\right). \tag{29}$$

In Fig. 12 we present our DNS data in terms of both

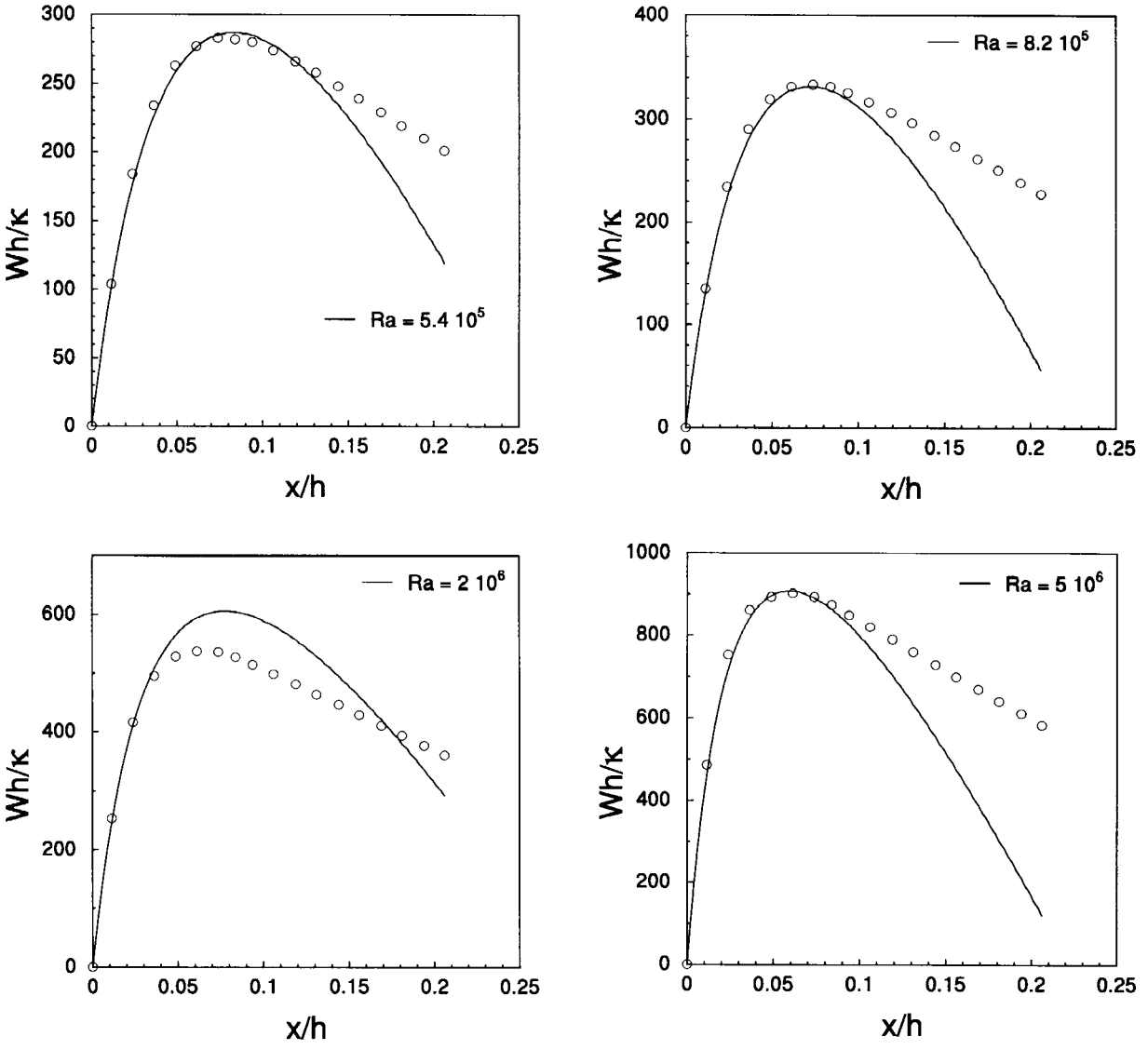

Fig. 13. The velocity profile in the inner layer as expressed by a wall function relationship (solid line) and the DNS data (symbols) for $Ra = 5.4 \times 10^5$ (upper left), $Ra = 8.2 \times 10^5$ (upper right), $Ra = 2 \times 10^6$ (lower left) and $Ra = 5 \times 10^6$ (lower right).

scaling relationships (28) and (29). The results show that in view of the large variation of the velocity found in Fig. 4, the DNS data collapse quite well onto a single curve both in the inner and outer layer. This is in particular the case for the outer layer where it seems that the scale mean velocity gradient can be very well described by a constant value.

Let us now consider the matching of both expressions (28) and (29). Because the velocity gradient in the inner layer is formulated in terms of a defect law, we can apply our matching arguments only to the second derivative of the velocity. Using standard arguments for matching as discussed in Section 4.2, we find that the following matching relationship for the velocity gradient should apply

$$\frac{\mathrm{d}\bar{w}/\mathrm{d}x\,|_0 - \mathrm{d}\bar{w}/\mathrm{d}x}{w_\mathrm{i}/l_\mathrm{i}} = -c_3\left(\frac{x}{l_\mathrm{i}}\right)^{-2/3} + A_2$$

$$\frac{\mathrm{d}\bar{w}/\mathrm{d}x}{w_\mathrm{o}/h} = c_3\left(\frac{x}{h}\right)^{-2/3} + B_2. \tag{30}$$

We expect this matching result to apply in more or less the same region as the matching we have found for the Reynolds stress (see Fig. 10). However, we could not

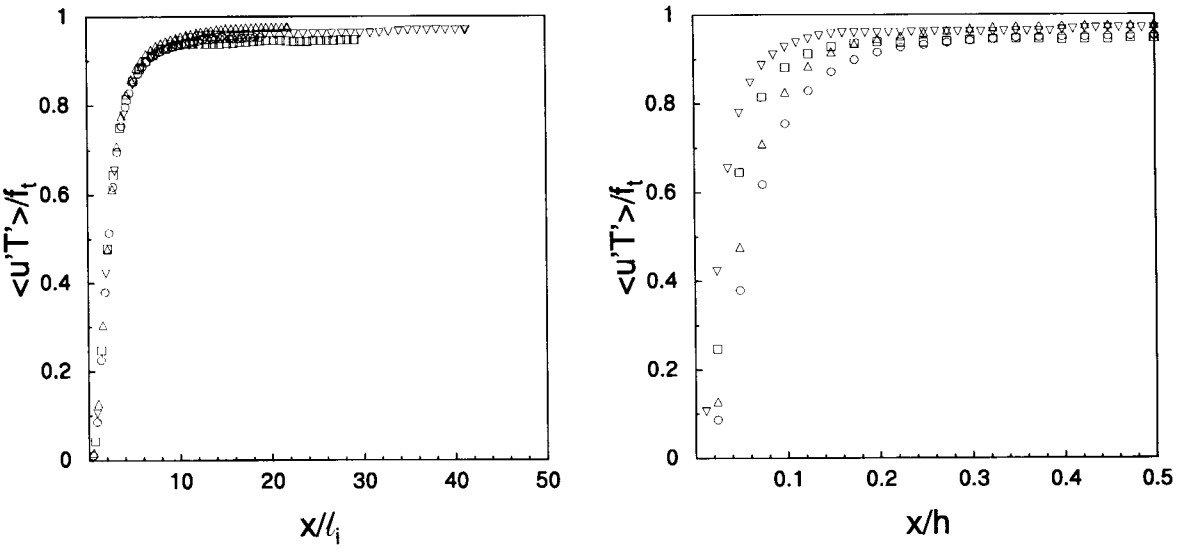

Fig. 14. DNS data for the horizontal temperature flux in inner-layer scaling (left) and outer-layer scaling (right); the meaning of the symbols is given in Table 2.

find in this region, a convincing fit by means of (30) to the DNS data. A reason for this failure may perhaps be that the matching region is still too small. Namely, although the Rayleigh number may seem very high, it should be realised that in view of the background of DNS our results are representative of only very low-Reynolds number turbulence. Therefore, the limit $h/l_i \to \infty$ may not be very well satisfied. Another unresolved issue is an inconsistency between the inner and outer velocity gradient in the matching region. In the matching region the relations (30) should lead to the same velocity gradients. However, the inner layer formulation (28) suggest that the velocity gradient in the matching region is $O(H)$ whereas (30) for the outer layer leads to $O(H^{4/9})$ for the velocity gradient. Therefore, despite the convincing scaling behaviour of expressions (28) and (29) as shown in Fig. 12 we must consider scaling for the mean velocity as being not completely solved.

Nevertheless, the excellent scaling shown in Fig. 12 can be exploited to reconstruct the velocity profile by integration of the expressions (28) and (29). Let us concentrate on the velocity profile in the inner layer. A direct integration of (28) in dimensional notation leads to

$$w = \left.\frac{\mathrm{d}\bar{w}}{\mathrm{d}x}\right|_0 x - w_i f_w\left(\frac{s}{l_i}\right). \tag{31}$$

An expression for f_w which seems to give a reasonable fit to the DNS data of the velocity in the inner layer, is found to be

$$w = \left.\frac{\mathrm{d}\bar{w}}{\mathrm{d}x}\right|_0 x - w_i \frac{C_1\left(\frac{x}{l_i}\right)^2}{C_2 + \left(\frac{x}{l_i}\right)} \tag{32}$$

where for the constants, the following values have been found: $C_1 = 9.7$, and $C_2 = 2.8$.

The fit of (32) to the DNS data is shown in Fig. 13. The agreement is indeed quite reasonable which again can be considered as indirect proof for the scaling as proposed in (28). For $Ra = 2 \times 10^6$ the agreement is not as good as for the other three cases. The deviation between (32) and the DNS data can be traced back to the value of the velocity gradient at the wall, i.e. $\mathrm{d}\bar{w}/\mathrm{d}x|_0$. Only an error of 3% in this gradient is sufficient to explain the deviation found in Fig. 13. In any case the results shown in Fig. 13 are sufficiently encouraging to propose (32) as a wall function for the mean velocity.

5. Scaling of turbulence quantities

In this section we consider the scaling of various second moments of turbulence quantities. Our point of departure is again a scaling in terms of an inner- and an outer-layer as we have used in the previous section.

5.1. Temperature flux

Let us first consider the horizontal temperature flux $\overline{u'T'}$. We have argued in Section 4.1 that the total horizontal temperature flux, f_t given by (9), is constant and

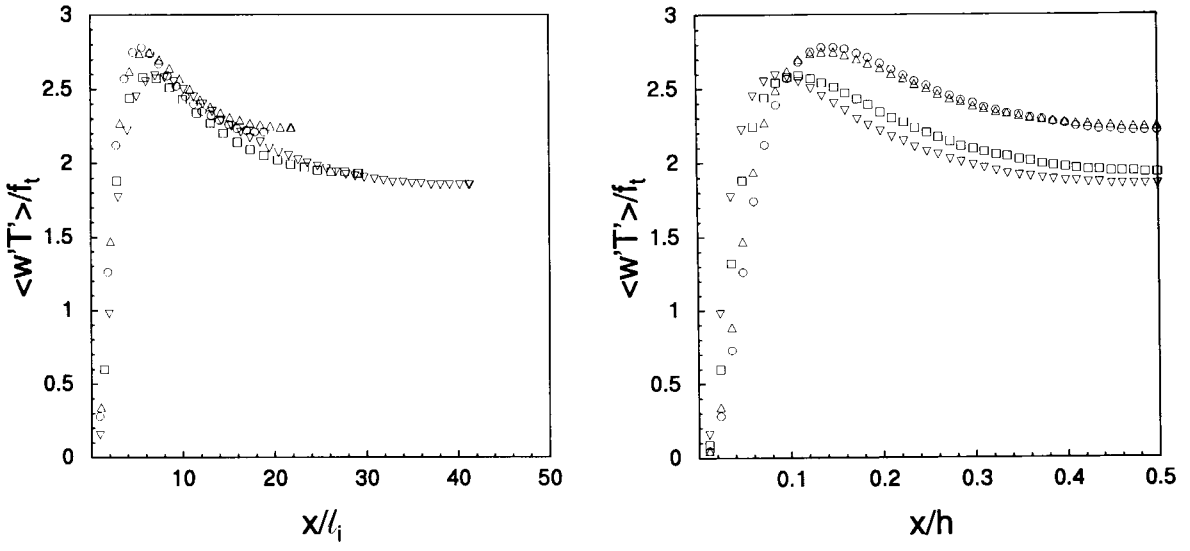

Fig. 15. DNS data for the vertical temperature flux in inner-layer scaling (left) and outer-layer scaling (right); the meaning of the symbols is given in Table 2.

we have proposed f_t as a characteristic scaling parameter. Moreover, we have found in Section 4.2 that the temperature profile can be scaled in terms of an inner and outer layer where f_t is used in both layers as a characteristic scaling parameter. In view of (9), the horizontal temperature flux should also allow scaling in terms of an inner and outer layer given, respectively, by

$$\frac{\overline{u'T'}}{w_i T_i} = g_{u\theta}\left(\frac{x}{l_i}\right) \tag{33}$$

$$\frac{\overline{u'T'}}{w_o T_o} = G_{u\theta}\left(\frac{x}{h}\right). \tag{34}$$

These scaling relationships are shown in Fig. 14 for

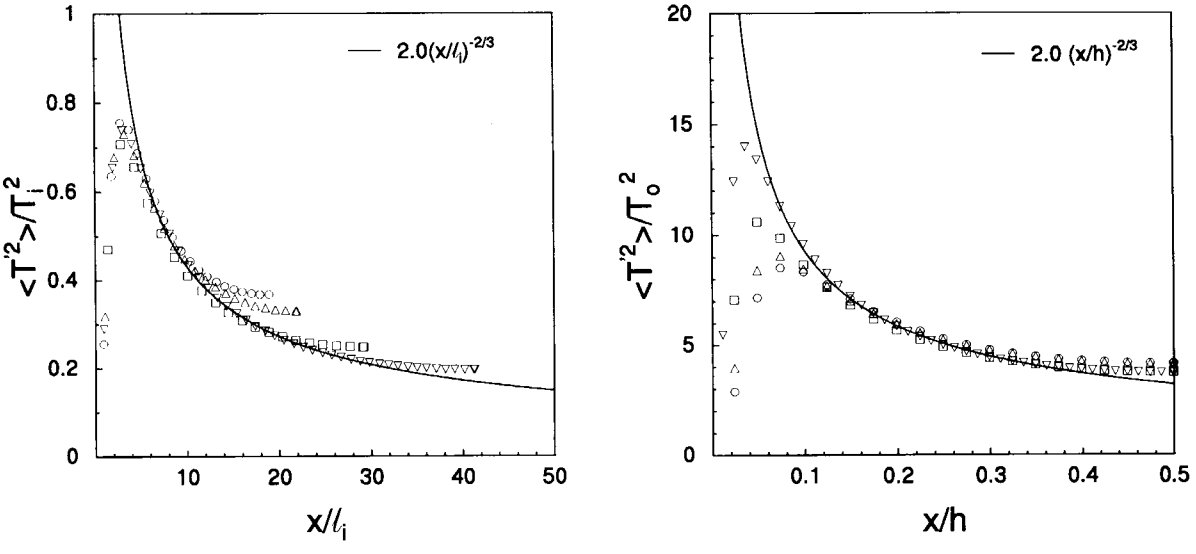

Fig. 16. DNS data for the temperature variance in inner-layer scaling (left) and outer-layer scaling (right); the meaning of the symbols is given in Table 2.

our DNS data and it is clear that the scaling is very well followed.

We note that both $w_i T_i$ and $w_o T_o$ are, by definition, equal to f_t. In other words the scaling of the temperature fluid in the inner and outer layer is the same. Matching of the inner and outer layer in an overlap region then leads to the result that both $g_{u\theta}$ and $G_{u\theta}$ should become equal to a constant. Fig. 14 shows that this matching behaviour is indeed reasonably well followed.

Next we consider the vertical temperature flux. The scaling of this quantity is not as straightforward as for the horizontal flux. The most reasonable assumption seems to be that the vertical flux should scale in the same way as the horizontal flux or alternatively that the ratio of the horizontal to the vertical flux should become a constant, i.e. independent of *Ra*. Although reasonable, it should be stressed that a real argument for this assumption is lacking. Nevertheless continuing, we find that the vertical temperature flux in the inner and outer layer should scale, respectively, as

$$\frac{\overline{w'T'}}{w_i T_i} = g_{w\theta}\left(\frac{x}{l_i}\right) \tag{35}$$

$$\frac{\overline{w'T'}}{w_o T_o} = G_{w\theta}\left(\frac{x}{h}\right). \tag{36}$$

These scaling relationships are given for our DNS data in Fig. 15. Although the scaling for $w'T'$ is not as clear as for $u'T'$, there are at present no arguments to propose another scaling.

5.2. Temperature variance

For the temperature variance we expect the same scaling to hold as for the mean temperature itself. This means that the temperature variance in the inner and outer layer can be expressed as

$$\frac{\overline{T'^2}}{T_i^2} = g_\theta^2\left(\frac{x}{l_i}\right) \tag{37}$$

$$\frac{\overline{T'^2}}{T_o^2} = G_\theta^2\left(\frac{x}{h}\right). \tag{38}$$

These scaling relationships are illustrated in Fig. 16 for our DNS data. It is clear that the scaling given by (37) and (38) is very well followed.

Matching the expressions (37) and (38) in the overlap region leads to the following explicit profiles for the temperature variance

$$\frac{\overline{T'^2}}{T_i^2} = c_4\left(\frac{x}{l_i}\right)^{-2/3} \tag{39}$$

$$\frac{\overline{T'^2}}{T_o^2} = c_4\left(\frac{x}{h}\right)^{-2/3} \tag{40}$$

in both the inner and outer layers, respectively. These matching expressions are also shown in Fig. 16. It is clear that for $c_4 = 2.0$ these expressions give an excellent fit to the data for the temperature variance for $x/l_i > 7$ and $x/h < 0.3$.

5.3. Velocity variances

Let us now turn to the variance of the velocity fluctuations. Scaling in terms of w_i and w_o seems to be the natural choice. However, let us first consider the budget equation of turbulent kinetic energy. For stationary and for homogeneous conditions in the y- and z-direction, this equation in non-dimensional form reads [23]

$$0 = -\overline{u'w'}\frac{d\bar{w}}{dx} + H\overline{w'\theta'} + T_e - \epsilon \tag{41}$$

where the first two terms on the right-hand-side are, respectively, the turbulence production by shear and by buoyancy. The T_e stands for the transport term which describes the transport of kinetic energy by velocity and pressure fluctuations. The ϵ denotes the energy dissipation.

We consider first the outer layer. Our DNS results show that here T_e is in general, small with respect to the production terms and can thus be neglected in the order-of-magnitude estimate needed fora scaling. The resulting equation then expresses a balance between the dissipation and the two production terms by shear and buoyancy, respectively. For the production terms we can obtain an order-of-magnitude estimate based on the scaling results that we have discussed in the previous section. For the outer layer we find for the shear and buoyant production, respectively,

$$-\overline{u'w'}\frac{d\bar{w}}{dx} \simeq H \cdot Nu \tag{42}$$

$$H\overline{w'\theta'} \simeq H \cdot Nu \tag{43}$$

which means that both production processes are equally important and consistent with our discussion on the scaling of the Reynolds-stress and temperature integral given in the outer layer in Section 4.3. Let us now introduce a velocity scale for the turbulence by means of the dissipation which can be estimated as

$$\epsilon \simeq \frac{\mathscr{U}_o^3}{h}. \tag{44}$$

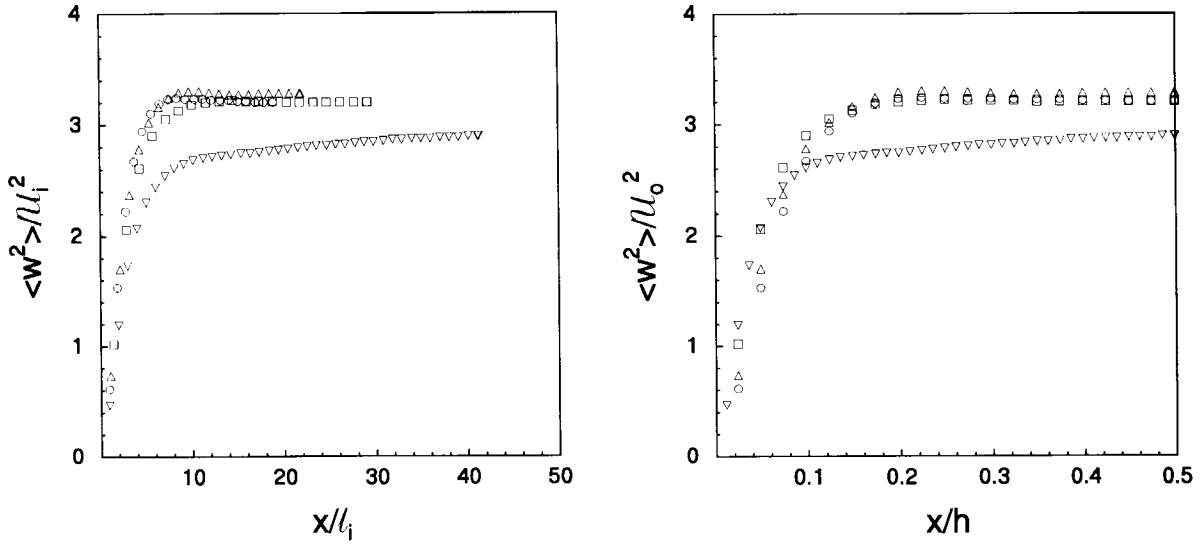

Fig. 17. DNS data for the vertical velocity variance, $\overline{w'^2}$ in inner-layer scaling (left) and outer-layer scaling (right); the meaning of the symbols is given in Table 2.

Equating (44) with the scaling estimates (42) and (43) for the production terms leads to

$$\mathscr{U}_o \simeq (H\,Nu)^{1/3}. \tag{45}$$

According to the results given in Table 3, this implies that the scaling velocity $\mathscr{U}_o$ is equal to the velocity scale w_o.

Next we consider the inner layer. Here the choice for the correct velocity scale is more complicated because results presented by Boudjemadi et al. [12] and by Versteegh and Nieuwstadt [22] show that in this region the energy budget cannot be described by a simple balance between production and dissipation. For instance, as we have argued in Section 3, shear production in the near-wall region is negative. A major source of turbulence here is the transport term T_e.

Let us assume that this transport term can be scaled in terms of the velocity scale $\mathscr{U}_o$ in the outer layer and in terms of the inner velocity scale $\mathscr{U}_i$ in the near-wall

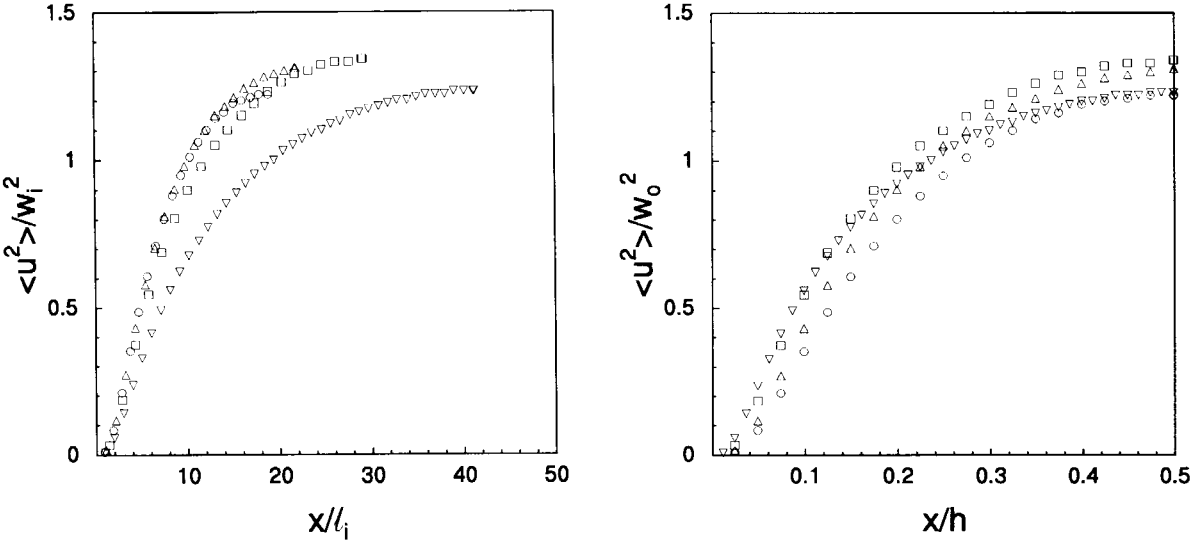

Fig. 18. DNS data for the horizontal velocity variance, $\overline{u'^2}$ in inner-layer scaling (left) and outer-layer scaling (right); the meaning of the symbols is given in Table 2.

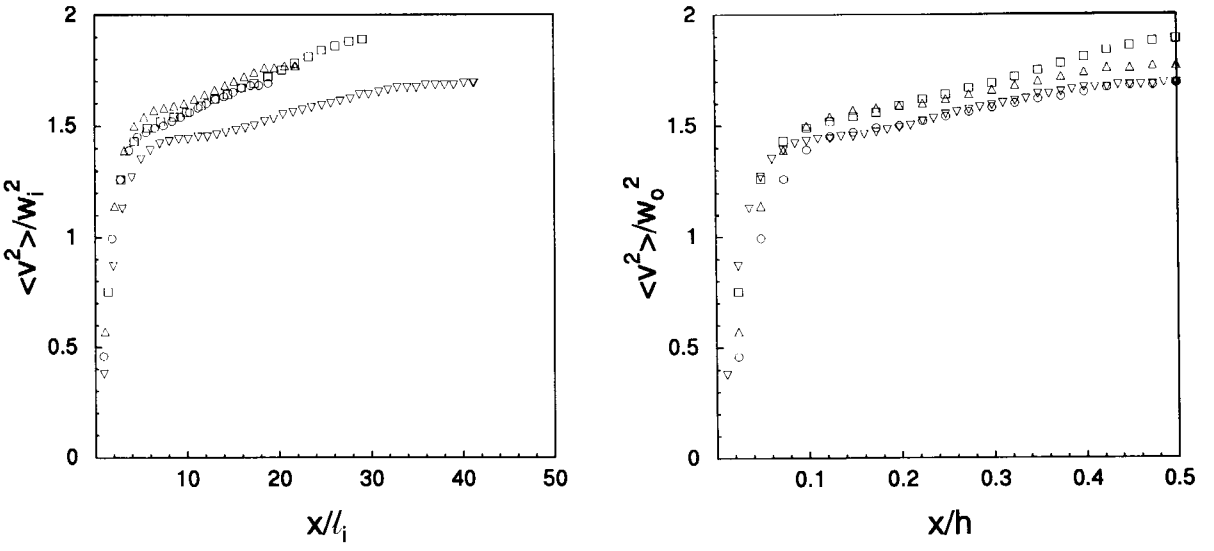

Fig. 19. DNS data for the horizontal velocity variance, $\overline{v'^2}$ in inner-layer scaling (left) and outer-layer scaling (right); the meaning of the symbols is given in Table 2.

inner region. As a result the composite expression for T_e in dimensional notation becomes

$$T_e = \frac{\mathscr{U}_i^3}{l_i} g_{T_e}\left(\frac{x}{l_i}\right) + \frac{\mathscr{U}_o^3}{l_i} G_{T_e}\left(\frac{x}{h}\right)$$

where we have omitted the subtraction of the matching expression. Next we apply the constraint that when integrated across the channel, the integral of the transport term should, by definition, become zero. Consequently, we find

$$0 = \mathscr{U}_i^3 \int_0^\infty g_T(\xi)\,\mathrm{d}\xi + \mathscr{U}_o^3 \int_0^{0.5} G_T(s)\,\mathrm{d}s$$

with the result that

$$\mathscr{U}_i \equiv \mathscr{U}_o.$$

The turbulence velocity scale in the inner layer is thus equal to the velocity scale in the outer layer. This equality of the two velocity scales implies that the matching between the inner and outer layer results in a constant value for the scaling function in the matching region. Based on these results we shall consider the scaling of the various velocity variances below.

We first consider the scaling of the vertical velocity variance $\overline{w'^2}$ which for the inner and outer layer reads

$$\frac{\overline{w'^2}}{\mathscr{U}_i^2} = g_{w^2}\left(\frac{x}{l_i}\right) \tag{46}$$

$$\frac{\overline{w'^2}}{\mathscr{U}_o^2} = G_{w^2}\left(\frac{x}{h}\right). \tag{47}$$

These expressions are illustrated in Fig. 17 in terms of our DNS data. Except for the highest Rayleigh number case our scaling approach works reasonably well in collapsing the data onto a single curve. Also the matching in terms of a constant value for the functions g_{w^2} and G_{w^2} seems reasonably well followed.

The scaling results for the variance of the two horizontal velocity components are illustrated in Figs. 18 and 19. Again the behaviour of the data for the highest Rayleigh number differs from the results for the other Rayleigh numbers. With respect to the scaling one could say that in comparison with the original data for these variances shown in Figs. 5 and 6 the scaled data seem to collapse reasonably well. However, it is also clear that the scaling behaviour for these horizontal variances seems to be slightly worse than for the case of the vertical variance. Also the matching results which implies a constant value in the matching region, is not very well followed especially for the $\overline{u'^2}$ variance. Nevertheless, at this stage we have no other evidence which would justify the introduction of another scaling for the horizontal variances.

6. Summary and conclusions

By means of a DNS we have studied the natural convection flow between two infinite differentially heated vertical walls. Computations have been carried out for a Rayleigh number which varies between

5.4×10^5–5×10^6. The DNS results agree well with the experimental data obtained by Dafa'Alla and Betts [6] in a tall cavity.

The main objective of our investigation has been to study the scaling behaviour of this natural convection flow and based on the scaling to propose wall functions. The point of departure has been the study by George and Capp [17] who define an inner and outer layer and propose a scaling relationship for the mean temperature and mean velocity in these layers. Based on a matching of these inner and outer scaling relationships an explicit expression for the mean profile in the matching region is found. In addition a transfer law can be derived by combining the inner- and outer-layer profiles in the matching region. For the mean temperature these scaling results are in excellent agreement with our DNS data. This can be considered as confirmation of previous studies based on experimental data in which temperature profiles have been found to scale according to relationships proposed by George and Capp [17].

The scaling of the mean velocity profile has proved to be more difficult and the scaling expressions for this variable suggested by George and Capp [17] have not been confirmed by experiments. Therefore, we look for an alternative scaling approach. For this we turn to the equation of motion for the mean vertical velocity. Based on an order-of-magnitude analysis of all the terms in this equation we find that the near-wall region is governed by a balance between the viscous stress and the buoyancy term. Based on this result we propose a scaling of the mean velocity profile in terms of a defect law for the mean velocity gradient in the inner layer. In the outer layer the velocity gradient is found to scale in terms of the standard velocity scale introduced by George and Capp [17]. This new scaling agrees quite well with the DNS data. However, no clear matching between the inner and outer layer profile could be found and, moreover, the formulation of the inner and outer layer profile does not seem to be completely consistent. Nevertheless, the good agreement of scaling results with the DNS data allows us to propose a wall function for the near-wall velocity which can be used to prescribe a profile for this velocity.

We have also considered the scaling of several turbulence variables. The Reynolds stress and the temperature variance are found to scale in an inner and outer layer in terms of scaling variables introduced by George and Capp [17]. The same scaling applies to the horizontal temperature flux. This latter result is perhaps not so surprising because the (total) temperature flux which is constant across the channel, has been selected as one of the scaling parameters. A similar scaling approach for the vertical heat flux is not as convincing. However, it is not clear whether this variable should be scaled in terms of other variables. Finally, we have considered the scaling of the variances of the turbulent velocity fluctuations. Based on an analysis of the kinetic energy budget we have formulated an appropriate velocity scale valid in the inner and outer layer. It turns out that in both regions the velocity scales are equal to the outer velocity scale proposed by George and Capp [17]. The DNS data for the velocity variances confirm this scaling especially for the vertical velocity component.

At the start of this study, one could have perhaps expected that the scaling of this natural convection flow could be treated equivalently to the scaling of standard near-wall turbulent shear flows where one also distinguishes between an inner and outer layer. The scaling of the mean temperature profile seems to support this expectation. However, the results based on our DNS that we have presented here, show that this is not the case of the velocity profile and also for the velocity variances. Although the concept of an inner and outer layer seems to remain valid, we have found especially that the inner layer requires another scaling than what we would have expected from the standard scaling approach. For the mean velocity this results in a scaling relationship according to a defect law for the velocity gradient and for the velocity variance in the introduction of an alternative inner velocity scale. Therefore, we must conclude that this natural convection flow may perhaps seem simple in terms of flow geometry, its physics and therefore, its scaling behaviour appears to be far from simple.

Acknowledgement

The authors are indebted to Dr P. L. Betts for providing the experimental data and for discussions on the comparison between the experiments and the DNS.

References

[1] R.A. Antonia, M. Teitel, J. Kim, L.W.B. Browne, Low-Reynolds number effects in a fully developed turbulent channel flow, J. Fluid Mech. 236 (1992) 579–608.

[2] A. Chait, S.A. Korpela, The secondary flow and its stability for natural convection in a tall vertical closure, J. Fluid Mech. 200 (1989) 189–216.

[3] R.M. Kerr, Rayleigh number scaling in numerical convection, J. Fluid Mech. 310 (1996) 139–179.

[4] J.W. Elder, Laminar free convection in a vertical slot, J. Fluid Mech. 23 (1965) 77–97.

[5] P.L. Betts, A.A. Dafa'Alla, Turbulent buoyant air flow in a tall rectangular cavity, Proceedings of the ASME Meeting HTD 60 (1986) 83–91.

[6] A.A. Dafa'Alla, P.L. Betts, Experimental study of tur-

bulent natural convection in a tall cavity, Exp. Heat Transfer 9 (1996) 165–194.
[7] R. Cheesewright, Natural convection from a plane, vertical surface in non-isothermal surroundings, J. Heat Transfer 90 (1968) 1–8.
[8] T. Tsuji, Y. Nagano, Characteristics of a turbulent natural convection boundary layer along a vertical flat plate, Int. J. Heat Mass Transfer 31 (1988) 1723–1734.
[9] T. Tsuji, Y. Nagano, Turbulence measurements in a natural convection boundary layer along a vertical flat plate, Int. J. Heat Mass Transfer 31 (1988) 2101–2111.
[10] T. Tsuji, Y. Nagano, Velocity and temperature measurements in a natural convection boundary layer along a vertical plate, Exp. Thermal Fluid Sci. 2 (1989) 208–215.
[11] J.R. Phillips, Direct simulations of turbulent unstratified natural convection in a vertical slot for $Pr = 0.71$, Int. J. Heat Mass Transfer 39 (1996) 2485–2494.
[12] R. Boudjemadi, V. Mapu, D. Laurence, P. Le Quere, Budgets of turbulent stresses and fluxes in a vertical slot natural convection flow at Rayleigh $Ra = 10^5$ and 5.4×10^5, Int. J. of Heat Fluid Flow 18 (1997) 70–79.
[13] P. Bradshaw, G.P. Huang, The law of the wall in turbulent flow, Proceedings Roy. Soc. Lond., A 451 (1996) 165–188.
[14] D. Angirasa, F.T.M. Nieuwstadt, The mean temperature profile and the flux-profile relation in turbulent thermal convection, Int. Comm. Heat Mass Transfer 19 (1992) 395–408.
[15] F.T.M. Nieuwstadt, Turbulence and similarity theory in meteorology and engineering, in: A.A.M. Holtslag, P.G. Duynkerke (Eds.), Proceedings of the Colloquium Clear and Cloudy Boundary Layer, Kun. Ned. Acad. Science, 1998, pp. 43–66.
[16] B. Castaing, G. Gunaratne, F. Heslot, L. Kadanoff, A. Libchaber, S. Thomae, X-Z. Wu, S. Zaleski, G. Zanetti, Scaling of hard thermal turbulence in Rayleigh–Bénard convection, J. Fluid Mech. 204 (1989) 1–30.
[17] W.K. George, S.P. Capp, A theory for natural convection turbulent boundary layers next to heated vertical surfaces, Int. J. Heat Mass Transfer 22 (1979) 813–826.
[18] R.A.W.M. Henkes, C.J. Hoogendoorn, Numerical determination of wall functions for the turbulent natural convection boundary layer, Int. J. Heat Mass Transfer 32 (1989) 157–169.
[19] X. Yuan, A. Moser, P. Suter, Wall functions for numerical simulation of turbulent convection along vertical plates, Int. J. Heat Mass Transfer 36 (1993) 4477–4485.
[20] T.A.M. Versteegh, Numerical simulation of turbulent natural convection between two infinite, differentially heated vertical plates. PhD thesis, Delft University of Technology, 1998.
[21] T.A.M. Versteegh, F.T.M. Nieuwstadt, Direct numerical simulation of natural convection between two infinite, differentially heated vertical walls, in: Proceedings of the International Symposium on Advances in Computation Heat Transfer, Cesme, Turkey, 1998, p. 330.
[22] T.A.M. Versteegh, F.T.M. Nieuwstadt, Turbulent budgets of natural convection in an infinite, differentially heated, vertical channel, Int. J. Heat Fluid Flow 19 (1998) 135–149.
[23] H. Tennekes, J.L. Lumley, A First Course in Turbulence, MIT, Cambridge, 1972.